Advances in Environmental Technology

Fabrication of highly reactive MgO-NPs-CaO-hydrous nanocomposite and its application for the removal of manganese from aqueous solution

K. Nkele[1, 2], L. Mpenyana-Monyatsi[1], V. Masindi[2, 3]

[1]*Department of Environmental, Water and Earth Science, Faculty of Science, Tshwane University of Technology, Pretoria, South Africa*
[2]*Magalies Water, Scientific Services, Research and Development Division, Brits, South Africa*
[3]*Department of Environmental Sciences, College of Agriculture and Environmental Sciences, University of South Africa (UNISA), Florida, South Africa*

ARTICLE INFO

ABSTRACT

Elevated concentrations of manganese (Mn) in drinking water notoriously impart colour, metallic taste, and other (eco)-toxicological effects to the final water quality at different point of use (POU). Specifically, levels in the range of ≥100 to 300 µg/L are prevalently known to be of grave concern. Herein, the efficacy of the Mg-$(OH)_2$-Ca-NPs nanocomposite, i.e., calcined dolomitic effects, and its application for the removal of Mn from contaminated river water was explored. The nanocomposite was synthesized through mechanochemical activation using vibratory ball milling and thermal activation to remove CO_2 and other volatile impurities. The one factor at a time (OFAAT) modality was used to fulfil the objectives of this study, specifically the effects of contact time, dosage, and mixing speed. To substantiate that, experimental results, state-of-the-art analytical techniques, and geochemical modelling (PHREEQC) were used to substantiate the study results. The optimum conditions were observed to be 15 min of mixing, 0.5 g of dosage, and 200 rpm of mixing speed. The interaction of Mn containing aqueous solution with hydrated lime (Ca$(OH)_2$) and magnesium oxide (MgO) as well as their nanocomposite, i.e., Mg-$(OH)_2$-Ca-NPs nanocomposite, led to an increase in the pH that registered as ≥11.87, ≥10.17, and ≥11.35, respectively. The Mn removal efficiency registered as ≥72.4%, ≥91.8%, and ≥83% for the hydrated lime, MgO, and Mg-$(OH)_2$-Ca-NPs nanocomposite, respectively, whilst their turbidities were recorded as ≤0.41 NTU, ≤3.50 NTU and ≤1.05 NTU. An increase in pH and other factors resulted in the attenuation of Mn as a different chemical species, i.e., birnessite, hausmannite, bixbyite, manganite, nsutite, pyrolusite, and rhodochrosite. Ca^{2+}, Mg^{2+}, and Mn^{2+} were predicted to exist as divalent species in aqueous solution. The nanocomposite demonstrated superior performance compared to individual materials. As such, findings from

*Corresponding author: Tel: 0722859461
E-mail: kgolofelon@magalieswater.co.za

this study confirmed the performance and effectiveness of the Mg-$(OH)_2$-Ca-NPs nanocomposite on the removal of Mn from real river water. This will go a long way in curtailing the impacts of Mn in drinking water and further afield.

1. Introduction

Rapid population growth has proportionally led to an increase in industrial development and demands for resources. Although these activities contribute greatly to the economy of most countries, they also contribute to the pollution of aquatic ecosystems and the environment as a whole due to the disposal of chemicals in the form of effluents [1,2]. The pollutants that come from these human activities consist of elevated concentrations of heavy metals that may pose challenges to the receiving environment [3-5]. The presence of heavy metals in discharged industrial effluents has frightened both public works and waterworks [6]. In the family of heavy metals, Mn is one of the problematic chemical species that pose challenges to water resources and organisms that thrive in it. Furthermore, Mn is a chemically active element that can simply oxidize, but this is dependent on the pH of the hosting waterbody. Essentially, Mn occurs naturally and is prevalent in rocks, the atmosphere, water, and soils [7]. Moreover, Mn also acts as a micronutrient that is of great importance for the maintenance of health as well as supporting the development and growth of living things, i.e., plants, humans, animals, and microorganisms, but this is up to a specific level and the degree of tolerance [7]. According to toxicological studies and epidemiological reports, Mn can result in toxicity in terrestrial and aquatic environments, especially when they are above acceptable limits or tolerance levels [8]. In plants and animals, it can cause neurotoxicity in Platyhelminthes, embryonic mortality, acute toxicity in fish, and a Mn-induced iron (Fe) deficiency in algae. In addition, it has different effects on terrestrial plants that have been specified by the World Health Organization [8]. [9] stated that high consumption of Mn from drinking water could lead to neurological disorders in humans. It has also been stated by [10] and [11] that if a significant amount of Mn accumulates in the brain, it may produce neurotoxicity and cause degenerative brain disorder (DBD). Children

exposed to high levels of Mn in drinking water may develop short-term memory loss and impaired attention, speed, and manual dexterity, as well as visual challenges, compared to children exposed to acceptable limits [12]. Prevalently, Mn removal in drinking water is mainly driven by aesthetic concerns, rather than public health issues [13]. However, the draft rule for the health-based standard of Mn developed by health Canada is 100 µg/L [14]. A health advisory developed by the United States Environmental Protection Agency (US EPA) for the level of Mn is 300 µg/L; it also has a secondary guideline of 50 µg/L for drinking water regarding aesthetic issues. The WHO has recommended ≤400 µg/L of Mn in drinking water. Specifically, Mn has been part of the effluent contaminants emanating from industrial activities, i.e., acid mine drainage, metallurgical houses, power production utilities, and other industries, presenting a worldwide environmental challenge [15,16]. These contaminants end up in waterways, causing devastating effects on users of downstream water resources. For this reason, treatment methods for the removal of Mn from aqueous solution have been developed: adsorption [17,18], precipitation/oxidation [13,17], filtration [13,17], ion exchange [17,19], bio-(phyto)-remediation [20], and crystallization [21]. These technologies have advantages and disadvantages, with adsorption having the challenge of quick saturation since most magnetic adsorbents utilized for the removal of heavy metals result in an adsorption capacity that is low [22]; filtration and ion exchange have the challenges of brine production and high energy demand. Bio-(phyto)-remediation require time, highly controlled environments, and space for effective performance. Crystallization generates salts that pose disposal costs if not properly managed. Lastly, precipitation is regarded as the best technology for concentrated and less concentrated solutions. It is advantageous due to its efficacy, availability of materials, less sophisticated nature, cheap costs of reagents, and easiness to implement. Alkaline based materials such as lime, hydrated lime,

brucite, periclase, soda ash, caustic soda, their tailings and carbonate derivatives are often used to remove Mn from aqueous solution. [23] evaluated the efficacy of limestone and lime for removing Mn from acidic mine drainage. The outcome of their study indicated that limestone and lime were effective in the removal of Mn, specifically at pH ≥10. Thenceforth, their slight difference indicated that lime was better in performance than limestone, which could be attributed to neutralisation capacity. Through lime addition, the produced volume of precipitate was 50% smaller compared to the volume generated by adding limestone. [24] evaluated the effect of aluminium sulphate and calcium oxide for the removal of Mn, colour, and Fe at peat water treatment. Their findings denoted the use of lime resulted in 100% Mn removal from the aqueous solution. [25] investigated passive in-situ remediation of metal-polluted water using caustic magnesia via the use of column assays. Their findings denoted a significant reduction in Mn from aqueous solution, i.e., 75 ppm to 0.04 ppm. In another study, [26] evaluated the removal of heavy metals from aqueous solution using precipitation as a mode of chemical attenuation. The removal efficacy was determined to be proportional to lime dosage, and the Mn was reduced from 1085 to 1.8 ppm (99% removal), specifically at pH 11.0. Furthermore, [27] evaluated the removal of phosphorus and heavy metals from waters using lime as a seeding material. In their study, the results indicated pH ≥10.5 to be adequate for the effective removal of Mn (100%). Similarly, [28] evaluated the use of amorphous magnesite and its calcined derivative for the removal of metals, including Mn, from aqueous solution. Results from their study denoted ≥99% removal efficacy for Mn from aqueous solution. [29] investigated the treatment of mineral processing effluent using magnesium oxide. Their results confirmed the superiority of MgO or periclase to lime when it came to the attenuation of heavy metals, e.g., Mn, Zn, Cu, and Pb. However, the use of MgO and hydrated lime materials as composite has never been employed. As such, this will be the first study in design and execution to explore the synthesis of Mg-$(OH)_2$-Ca-NPs nanocomposite for the removal of Mn from aqueous solution. Specifically, a facile approach of using thermo-mechano-chemical activation via vibratory ball milling and calcination was adopted. State-of-the-art facilities were used for optimisation and characterisation of the feedstocks.

2. Material and methods

2.1. Acquisition of the samples

Aqueous samples were collected from a water treatment plant (WTP) which receives water from the Wilge River. The river is located in Gauteng, South Africa (25°49′0″ S and 28°52′0″ E). The water samples were collected using 25 L containers for bulk experiments. As a quality control initiative, the sampling containers were thoroughly rinsed prior to sampling to avoid contamination. Hydrated lime and magnesium oxide samples were procured from Protea Chemicals Pty (Ltd), South Africa.

2.2. Synthesis (fabrication) of the nanocomposite

In this study, the mechano-chemical synthesis technique was utilised as the method for the synthesis of the highly reactive nanocomposite. This study adopted methods proposed by [30] to synthesize the bentonite clay-MgO-NPs nanocomposite, and the outcomes are envisaged in this study. Specifically, the MgO-NPs-CaO nanocomposite was synthesised using a vibratory ball mill. 500 g of MgO-NPs and hydrated lime were mixed at a 1:1 wt.% mass ratio. The mixture was crushed and homogenized for 30 minutes at 1600 rpm using a vibratory ball mill until particles of fine powder were acquired. After milling, the homogeneous sample was sieved ≤32 μm particle size. The sample was then sealed in a plastic bag until utilisation for Mn removal experiments.

2.3. Optimization studies

For the establishment of optimum conditions that are suitable for the removal of Mn from aqueous solution, several operational parameters were optimized, including time, dosage, and mixing speed. Specifically, batch experiments were conducted in the laboratory using one-factor-at-a-time (AFAAT). Detailed information and explanations of various operational parameters and conditions thereto are enumerated below. The removal efficiency (%) was calculated using the equation that follows [31]:

$$R = \frac{Co - Ce}{Co} \times 100 \qquad (1)$$

2.3.1. Effect of time

Precisely, a volume of 500 mL solution of raw water was added into six 1000 mL beakers, into which 0.5 g of the nanocomposite was subsequently added. The mixtures were mixed at 5, 10, 15, 20, 25, and 30 minutes at 250 rpm using a jar test stirrer. Thereafter, approximately 10 minutes of settling was observed. After settling, the samples were assessed for pH, electrical conductivity (EC), turbidity, and Mn concentration. Similar conditions and procedures were used for the MgO-NPs and hydrated lime. The experiments were conducted in triplicate, and the acquired results were reported as mean values.

2.3.2. Effect of dosage

Five hundred millilitres of the real sample were added into a series of six 1000 mL beakers. Thereafter, different masses of the MgO-NPs-CaO nanocomposite (0.5 – 3.0 g) were added into the beakers. The mixtures were agitated for an optimum time of 15 minutes at 250 rpm using an overhead stirrer mounted on a jar test stirrer. Thereafter, the samples were afforded 10 minutes for the suspended solids to settle. After settling, the samples were assessed for pH, EC, turbidity, and Mn concentration. Similar conditions and procedures were used for the MgO-NPs and hydrated lime.

2.3.3. Effect of mixing speed

Congruent to the effect of time and dosage, 500 mL of the real sample was added into a series of six 1000 mL beakers, into which 0.5 g of MgO-NPs-CaO-hydrous nanocomposite was also added. The mixtures were agitated for 15 minutes each at different mixing speeds, i.e., 50, 100, 150, 200, 250, and 300 rpm, using overhead stirrers mounted on a jar test stirrer. Thereafter, the samples were afforded 10 minutes for suspended solids to settle. After settling, the samples were assessed for pH, EC, turbidity, and Mn concentration. Similar conditions and procedures were used for MgO-NPs and hydrated lime.

2.4. Characterization

2.4.1. Aqueous sample characterization

After the optimisation studies and optimum conditions, the feed and product samples were characterised using a multimeter probe (Hach 40d 13995 pH401) for the determination of pH and EC. Most importantly, the calibration of the pH meter was done in accordance with the instructions of the manufacturer before each analysis to ensure accuracy and reliability in the obtained results. A spectrophotometer (DR 3900 Hach) was used for the determination of dissolved Mn. The reagents utilized for the determination of Mn were the PAN indicator, ascorbic acid powder pillow, and alkaline-cyanide. Similarly, a spectrophotometer (TL2350 Hach) was also used to determine turbidity, i.e., both raw and final (treated) water. As part of the inter-laboratory analyses and quality control, the main parameters of the collected aqueous samples were measured using standard and approved methods in a state-of-the-art laboratory at the Magalies Water, Scientific Services (ISO/IEC 17025:2017 accredited), Brits, North West, South Africa.

2.4.2. Solid samples characterization

To support and complement outcomes from aqueous experiments, the MgO-NPs, hydrated lime and their nanocomposite were characterized. Specifically, the elemental and microstructural properties, i.e., elemental mapping, spot analysis, morphology, metal functional groups, and elemental composition, were determined. In particular, the elemental composition was determined using X-ray fluorescence (XRF) (Thermo Scientific's ARL PERFORM'X Sequential XRF Spectrometer containing UniQuant softwater for standardless analysis). Microstructural and elemental properties were determined using Field Emission (FE) Scanning Electron Microscope (SEM) containing Focused-Ion Beam (FIB) coupled to Energy Dispersive X-ray Spectroscopy (EDS) (Zeiss Auriga FIB/FESEM/EDS). The functional group was determined using the Fourier Transform Infrared Spectrometer (FTIR) (PerkinElmer's Spectrum 100-FTIR instrument containing a PerkinElmer Precisely Universal Attenuated Total Reflectance (ATR) sampling accessory with a diamond crystal). Lastly, the mineralogical composition was

determined using X-ray diffraction (XRD) (Malvern Panalytical, Aeris Edition containing a PIXcel detector). The characterization of solid samples was done at the National Centre for Nanostructured Materials (NCNSM) Council for Scientific and Industrial Research (CSIR), South Africa.

2.5. Geochemical modelling

To complement experimental results, the PH REdox EQuilibrium (in C language) (PHREEQC) geochemical model was employed [32,33]. That was done to determine aqueous species and possible mineral phases that are likely to be generated from the interaction of the nanocomposite with Mn containing aqueous solution. This will then be used to substantiate some of the findings. SI=<1 denotes under-saturation, SI=0 denotes saturation, and SI>1 denotes super-saturations.

3. Results and discussions

3.1. Effect of contact time

The results on the effect of contact time on the removal of Mn from aqueous solution are illustrated in Figures 1(a–c) and 2. Various contact times, i.e., 5, 10, 15, 20, 25, and 30 in minutes, were examined, as mentioned in section 2.3.

Figure 1a shows the results of the effect of the Mg-$(OH)_2$-Ca-NPs nanocomposite, hydrated lime, and MgO-NPs on the removal of the contaminants. As depicted in Figure 1a, there was a decrease in Mn with an increase in contact time. In particular, the Mg-$(OH)_2$-Ca-NPs nanocomposite demonstrated the characteristics of the hydrated lime and MgO-NPs as shown in the graph. Specifically, MgO-NPs achieved ≥75% removal efficiency, while Mg-$(OH)_2$-Ca-NPs nanocomposite achieved ≥55% removal efficacy, and hydrated lime achieved ≥38% removal efficacy for Mn.
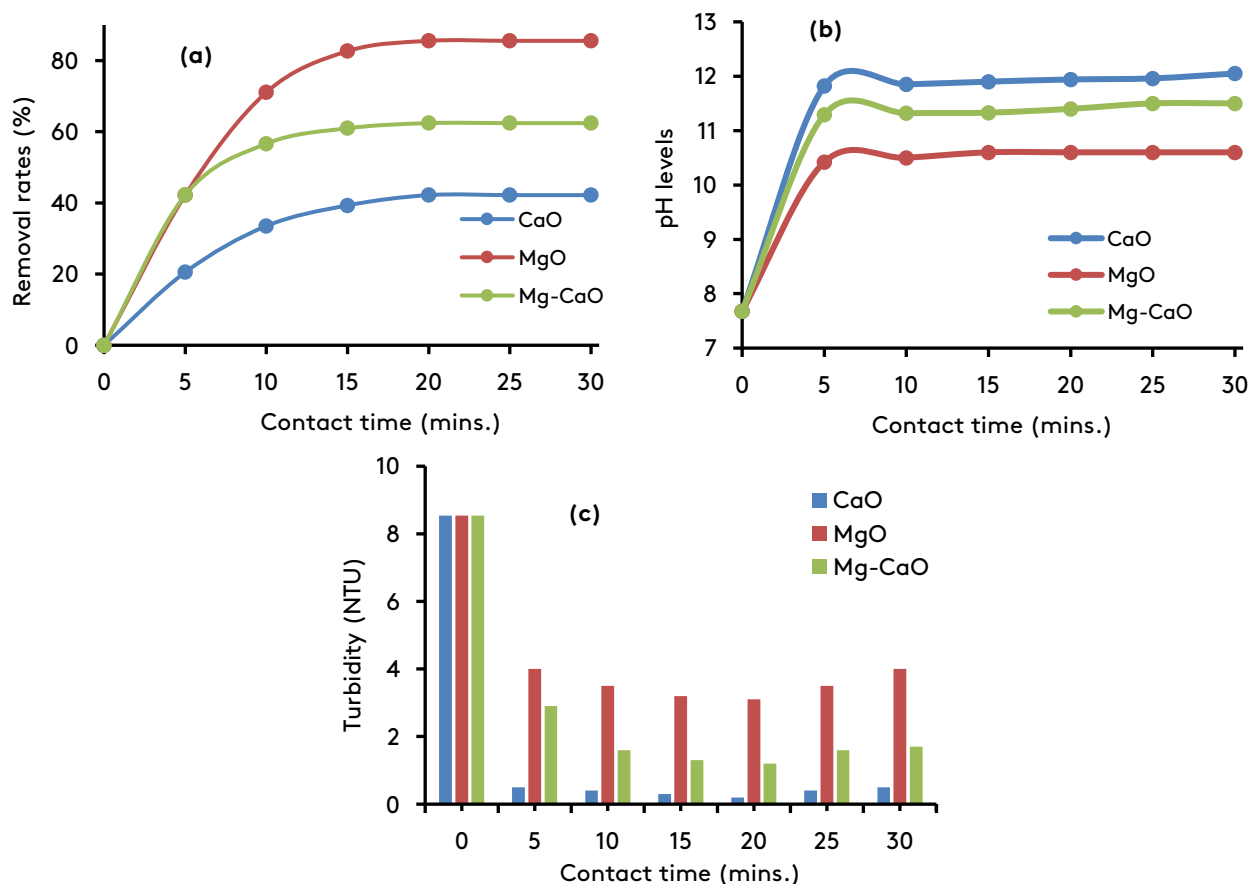
Fig. 1. Variation in the % removal of Mn (a), pH (b), and turbidity expressed in NTU (c) in aqueous solution as a function of time (Conditions: 0.5 g of each precipitant, 346 µg/L Mn^{2+}, 5 min time difference, 250 rpm, 10 min settling time).

Interestingly, the findings for the effect of MgO-NPs corroborate what has been reported by [34]. In their study, polyurethane was impregnated with MgO, and its efficacy on the removal of Mn from aqueous solution was evaluated. [35] Compared the efficiency of high-purity limestone, magnesite, quartzite, and dolomite as seeding materials for the removal of Mn. They reported the removal of Mn as manganese hydroxides with magnesite, dolomite, and limestone achieving ≥ 28% ≥ 32% ≥ 23%, respectively. The experimental outcomes in Figure 1b show the effectiveness of precipitating agents on pH as a function of contact time. As depicted in Figure 1b, the pH increased drastically between times 0 to 5 mins. Thereafter, there was a slow increase in pH with time. At the 30 mins interval, hydrated lime increased the pH to ≥12.0, while MgO-NPs increased the pH to ≥10.0, and, lastly, the Mg-$(OH)_2$-Ca-NPs nanocomposite increased the pH to ≥11.0. An increase in pH may be attributed to the addition of hydroxyl groups from the interlayers and matrices of hydrated lime, MgO-NPs, and their nanocomposite, i.e., Mg-$(OH)_2$-Ca-NPs nanocomposite. As expected, an increase in pH is directly linked to the reduction in the concentration of Mn from aqueous solution. The findings from this study corroborate what has been reported by other researchers [36,37]. Thenceforth, the obtained results denote a proportional relationship between pH and metals, i.e., Mn, concentration. In a study by [31], the effect of pH on the removal of Mn was reported. The authors recommended the pH ≥10.5 to be effective for the removal of Mn, specifically when using lime. In Figure 1c, the experimental results indicate a decrease in turbidity with an increase in contact time. Specifically, the turbidity of aqueous solution decreased significantly from 0 to 5 mins. Thereafter, a slight decrease in turbidity was observed, with the hydrated lime attaining ≤1.00 NTU, MgO-NPs attaining ≤3.00 NTU, and Mg-$(OH)_2$-Ca-NPs nanocomposite attaining ≤2.00 NTU. However, hydrated lime demonstrated superior performance on turbidity compared to other precipitating agents. A study by [38], whereby lime was used as a coagulant, also indicated that turbidity decreased with an increase in contact time.
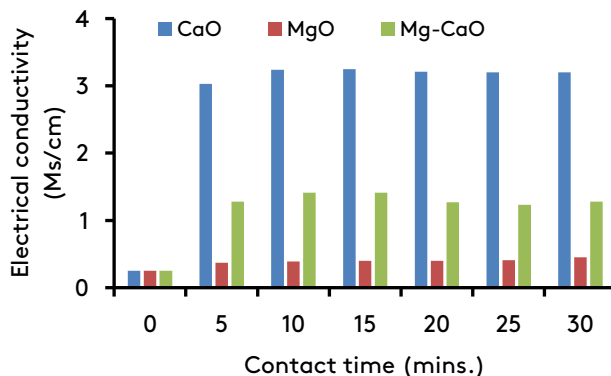
Fig. 2. Variations in electrical conductivity (EC) (mS/cm) as a function of contact time (Conditions: 0.5 g of individual precipitant, 346 µg/L of Mn^{2+}, 250 rpm, and 10 min of settling time).

EC is the ability of the aqueous solution to conduct electricity [39]. In this study, EC was found to increase with an increase in time (Figure 2). In particular, the hydrated lime showed a rapid increase in EC from 0 to 5 mins. Thereafter, no significant change in EC was observed. Specifically, the increase was ≥3.0, ≥0.4 mS/cm, and ≥1.0 for hydrated lime, MgO-NPs, and Mg-$(OH)_2$-Ca-NPs nanocomposite, respectively. Worryingly, hydrated lime increased EC to above the acceptable limit of 1.7 mS/cm, making the water unacceptable. Heed worthy, EC is the most useful tool to determine the purity of water in terms of dissolved ions [39]. As such, 15 minutes was taken as the optimum contact time for the removal of contaminants from aqueous solutions and was used in subsequent experiments.

3.2. Effect of dosage

The results of the effect of feedstock dosage on the removal of Mn from aqueous solution are reported in Figures 3(a–c) and 4. Various feedstock dosages, i.e., 0.5, 1.0, 1.5, 2.0, 2.5, and 3.0 in grams, were examined, as mentioned in section 2.3.
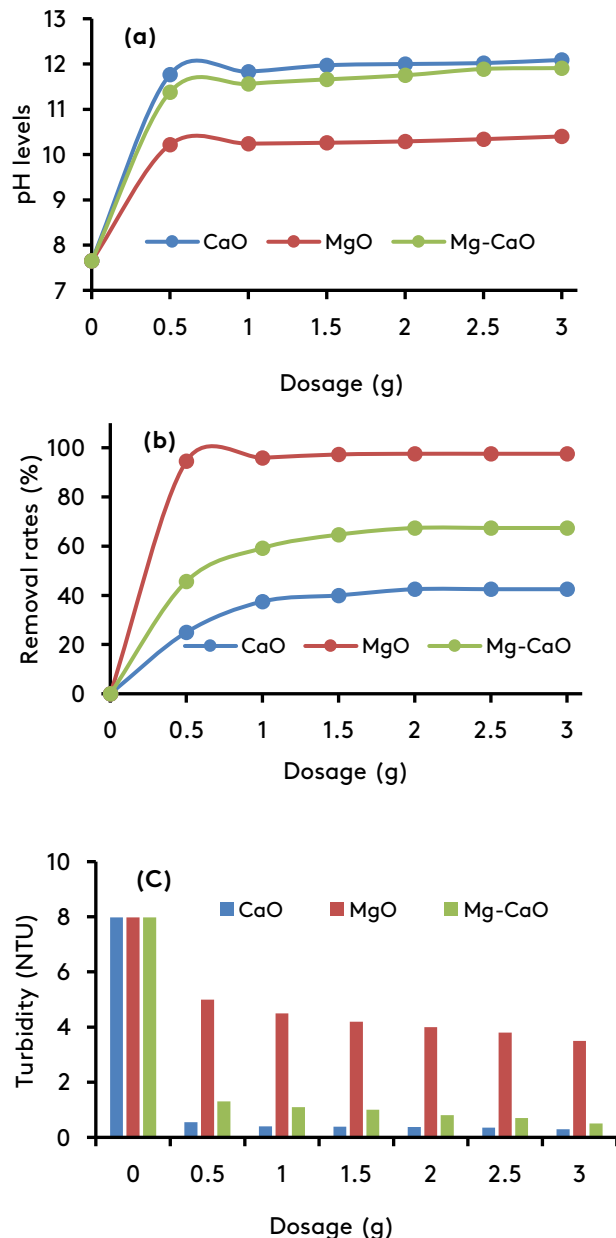
Fig. 3. Variation in the % removal of Mn (a), pH (b), and turbidity expressed in NTU (c) in aqueous solution as a function of feedstock dosage (Conditions: 15 minutes of mixing, 346 μg/L Mn^{2+}, 5 min time difference, 250 rpm, 10 min settling time).

As shown in Figure 3a, there was a variation in the percentage removal of contaminants as a function of dosage. Specifically, at 3 g, hydrated lime achieved ≥35% removal efficacy, MgO-NPs achieved ≥52% removal efficacy, and the nanocomposite achieved ≥39% removal efficacy. However, the MgO-NPs demonstrated greater strength on Mn attenuation compared to other chemicals. The obtained results corroborate what has been reported in the literature. [26] employed

lime for the removal of Mn from aqueous solution. Findings from their study demonstrated an increase in pH from 1.9 to 11.0 and a reduction in Mn levels from 1085 to 1.8 ppm. The experimental outcomes in Figure 3b showed the effectiveness of precipitating agents on pH as a function of feedstock dosage. As depicted in Figure 3b, there was an increase in pH with an increase in dosage, specifically from 0 to 0.5 g. Thereafter, no significant change in pH was observed. At the maximum dosage of 3 g, hydrated lime increased the pH to ≥12.0, while MgO-NPs increased the pH to ≥10.0, and the $Mg-(OH)_2-Ca$-NPs nanocomposite increased the pH to ≥11.0. An increase in pH may be attributed to the release of hydroxyl groups from matrices and interlayers of the hydrated lime, MgO-NPs, and $Mg-(OH)_2-Ca$-NPs nanocomposite. According to the literature [40-43], alkaline agents increase the pH, leading to the attenuation of metals through precipitation; a similar trend is anticipated and achieved in this study as well. In another study, [25] used caustic magnesia to increase the pH and attenuate metals. Their findings denoted the effective removal of Mn from aqueous solution using caustic magnesia, dead magnesia, or periclase (MgO). Furthermore, Figure 3c depicts a decrease in turbidity with an increase in the feedstock dosage. Specifically, the turbidity of the aqueous solution was significantly decreased by hydrated lime and $Mg-(OH)_2-Ca$-NPs nanocomposite, particularly between 0 to 0.5 g dosages. Thereafter, no change in turbidity reduction was observed. According to the results, the hydrated lime decreased the turbidity to ≤1.00 NTU, MgO-NPs to ≤5.00 NTU, and $Mg-(OH)_2-Ca$-NPs nanocomposite to ≤1.10 NTU. Apparently, the MgO-NPs denoted poor performance on the attenuation of turbidity. Interestingly, the results obtained for the effect of dosage using hydrated lime are supported by the report of [24], whereby ≥99% removal efficacy for Mn was achieved whilst the turbidity was decreased from 33.8 NTU to ≤1.90 NTU. Furthermore, the pH also increased from 3.1 to 7.1. Another study that supports these outcomes was performed by [44], whereby turbidity decreased with a decrease in the hydrated lime dosage. The turbidity decreased from 51700 NTU to 9000 NTU. Similar to the effect of contact time, findings from this experiment

further indicate an increase in EC with an increase in hydrated lime dosage (Figure 4).
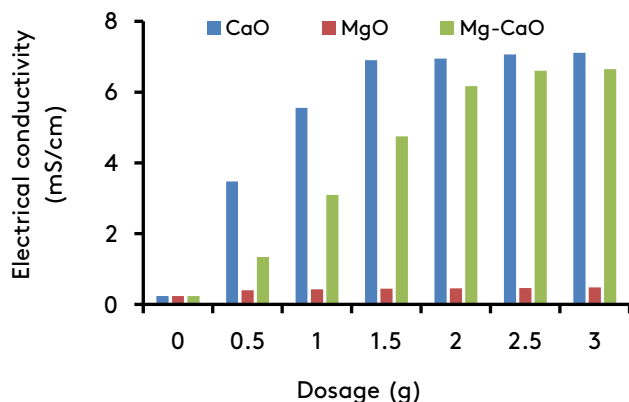
Fig. 4. Variations in electrical conductivity (EC) (mS/cm) as a function of feedstock dosage (Conditions: 15 minutes of mixing, 368 µg/L of Mn^{2+}, 250 rpm, and 10 min of settling time).

As shown in Figure 4, the EC of aqueous solution was found to be increasing with an increase in dosage. The hydrated lime and the Mg-$(OH)_2$-Ca-NPs nanocomposite significantly contributed to an increase in the EC of the product water, whilst the MgO-NPs contribution was trivial. Specifically, hydrated lime increased the EC from ≤0.20 to ≥7.00 mS/cm, MgO-NPs increased the EC to ≥0.40 mS/cm, and lastly, Mg-$(OH)_2$-Ca-NPs nanocomposite increased EC to ≥6.00 mS/cm. In a nutshell, 0.5 g was taken as the optimum dosage for this experiment and was used in subsequent experiments.

3.3. *Effect of mixing speed*

The results of the effect of mixing speed on the removal of Mn from aqueous solution are illustrated in Figures 5(a–c) and 6. Various mixing speeds, i.e., 50, 100, 150, 200, 250, and 300 in rpm, were examined, as mentioned in section 2.3. Figure 5a shows the results of the % removal of Mn as a function of mixing speed. Essentially, there was a reduction in the level of Mn as a function of mixing speed. At 300 rpm, the hydrated lime achieved ≥21% removal efficacy, MgO-NPs achieved ≥67% removal efficacy, and Mg-$(OH)_2$-Ca-NPs nanocomposite achieved ≥59% removal efficacy. The MgO-NPs demonstrated superior performance compared to the other chemicals. As expected, the pH of the product water increased with an increase

in the mixing speed (Figure 5b). Specifically, the pH increased drastically between speed 0 to 50 rpm. Thereafter, no significant change in pH was observed. At a speed of 300 rpm, which was the maximum speed, hydrated lime increased the pH to ≥11.0, the MgO-NPs increased it to ≥10.0 and the Mg-$(OH)_2$-Ca-NPs nanocomposite increased the pH to ≥11.0. Most importantly, the pH values acquired from these experiments were deemed suitable for the precipitation of Mn, and this was also confirmed by other studies in the literature [43,45-48]. Based on the results, 200 rpm was observed as the optimum condition for the removal of Mn from aqueous solution, and it was used in subsequent experiments. Figure 5c depicts the effect of mixing speed on turbidity of the final water. As expected, the turbidity decreased with an increase in mixing speed. The hydrated lime showed superior performance on turbidity as compared to the other chemicals. From 0-50 rpm, there was a rapid reduction in turbidity. Thereafter, no significant reduction in turbidity was observed. Specifically, the turbidity of the aqueous solution was significantly decreased by the hydrated lime and Mg-$(OH)_2$-Ca-NPs nanocomposite, especially from 0 to 50 rpm. Thereafter, no significant change was observed. Albeit, at 300 rpm, the MgO-NPs drastically decreased the turbidity to ≤3.00 NTU; the hydrated lime and the nanocomposite reduced the turbidity to ≤1.00 NTU. As shown in Figure 6, the EC of the aqueous solution was found to increase with an increase in the mixing speed. For hydrated lime, there was an extreme increase in EC from 0 to 150 rpm. Thereafter, there was a slight increase until 300 rpm. The MgO-NPs on the other hand remained almost constant throughout varying mixing speeds. Specifically, hydrated lime increased the EC from ≤0.30 to ≥3.00 mS/cm, the MgO-NPs increased the EC from ≤0.30 to ≥0.40 mS/cm and the Mg-$(OH)_2$-Ca-NPs nanocomposite increased EC from ≤0.30 to ≥1.00 mS/cm, hence confirming the dissolution of the chemical species from the matrices, micelle, and interlayers of the feedstocks. In light of the obtained results, 200 rpm was taken as the optimum mixing speed and was used in subsequent experiments.

(a)

(b)

(c)
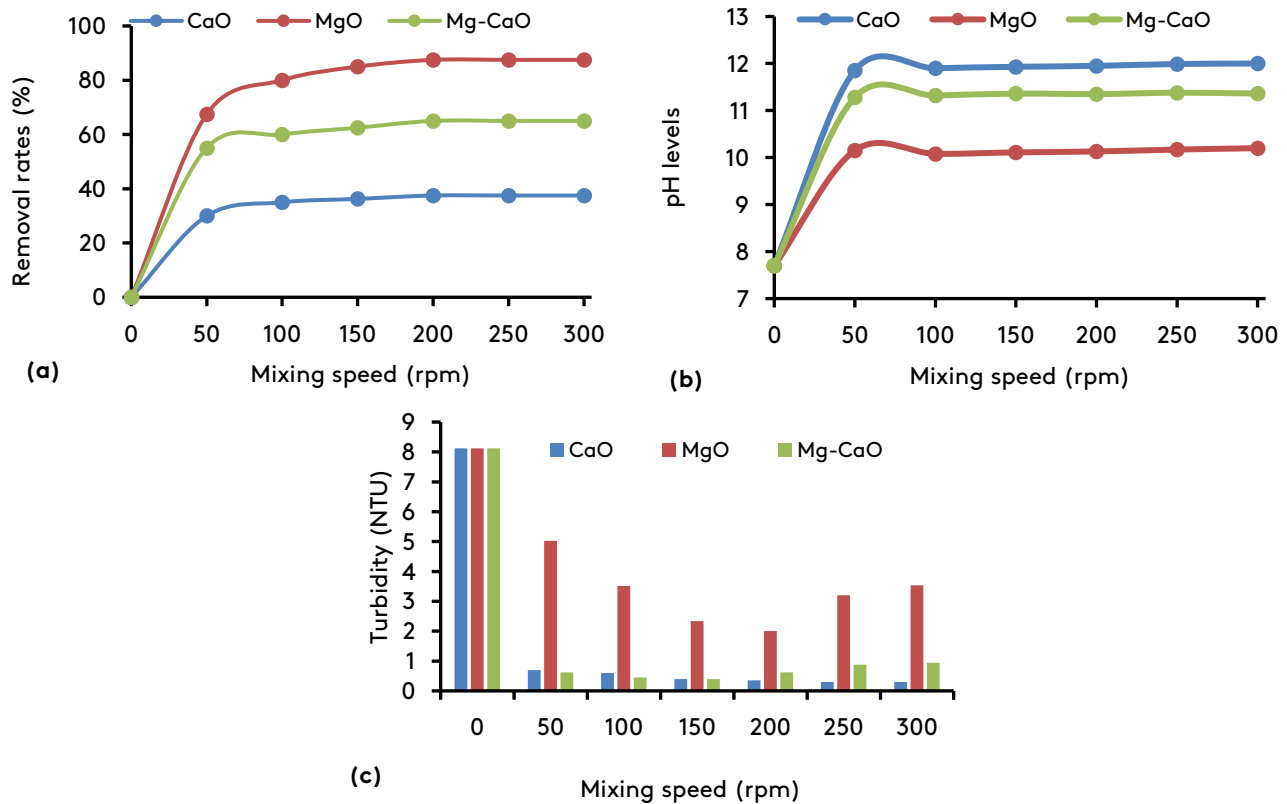
Fig. 5. Variation in the % removal of Mn (a), pH (b), and turbidity expressed in NTU (c) in aqueous solution as a function of mixing speed (Conditions: 15 minutes of mixing, 346 µg/L Mn^{2+}, 0.5 g of feedstock dosage, 10 min settling time).
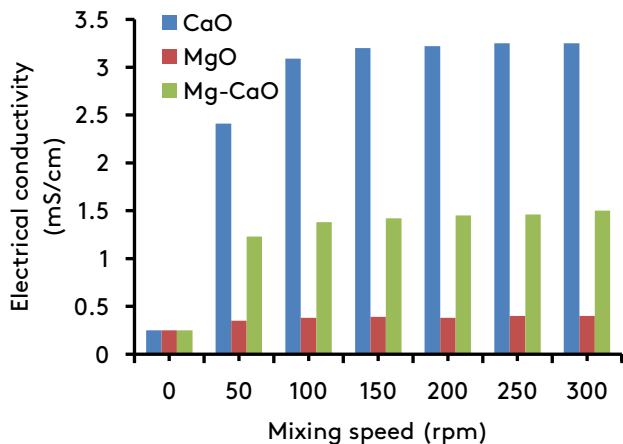
Fig. 6. Variations in electrical conductivity (EC) (mS/cm) as a function of mixing speed (Conditions: 15 minutes of mixing, 368 µg/L of Mn2+, 0.5 g of feedstock dosage, and 10 min of settling time).

4. Removal of Mn at optimised conditions

The results of the effect of hydrated lime, MgO-NPs, and their nanocomposite, i.e., Mg-(OH)$_2$-Ca-NPs nanocomposite, on Mn, turbidity, EC, and pH at optimised conditions are summarised in Table 1.

The experiments were conducted at 15 mins of mixing, 0.5 g of feedstock dosage, and 200 rpm of mixing speed. As shown in Table 1, the raw water had an elevated level of Mn, turbidity, and low pH and EC. However, after treatment, Mn was successfully removed by all the precipitating agents. However, the hydrated lime increased the EC of the product water to above the acceptable limits, as stipulated in SANS 241-2:2015 specifications. Hydrated lime was observed to be an excellent reagent for turbidity removal, while MgO-NPs were observed to be superior in terms of Mn removal. The synthesised nanocomposite denoted synergistic effects due to balanced attributes of individual materials and performances thereto. Thenceforth, this could be linked to the nanocomposite having the properties of the MgO-NPs and hydrated lime; hence it was noted to effectively remove Mn and turbidity resulting in the recorded dominance in performance as compared to individual materials.

Table 1. Summary of the effect of hydrated lime, MgO-NPs, and their nanocomposite on different parameters at optimised conditions.

Parameters	Units	Limits	Raw	Lime	MgO-NP	nanocomposite
Mn	μg/L	≤400	1000	276	82	170
%removal	-			72.4	91.8	83.0
Turbidity	NTU	≤1.00	8.21	0.41	3.50	1.05
%removal	-			95.0	57.4	87.2
pH	-	5-9.7	7.68	11.87	10.17	11.35
EC	mS/cm	≤1.70	0.25	3.31	0.39	1.39
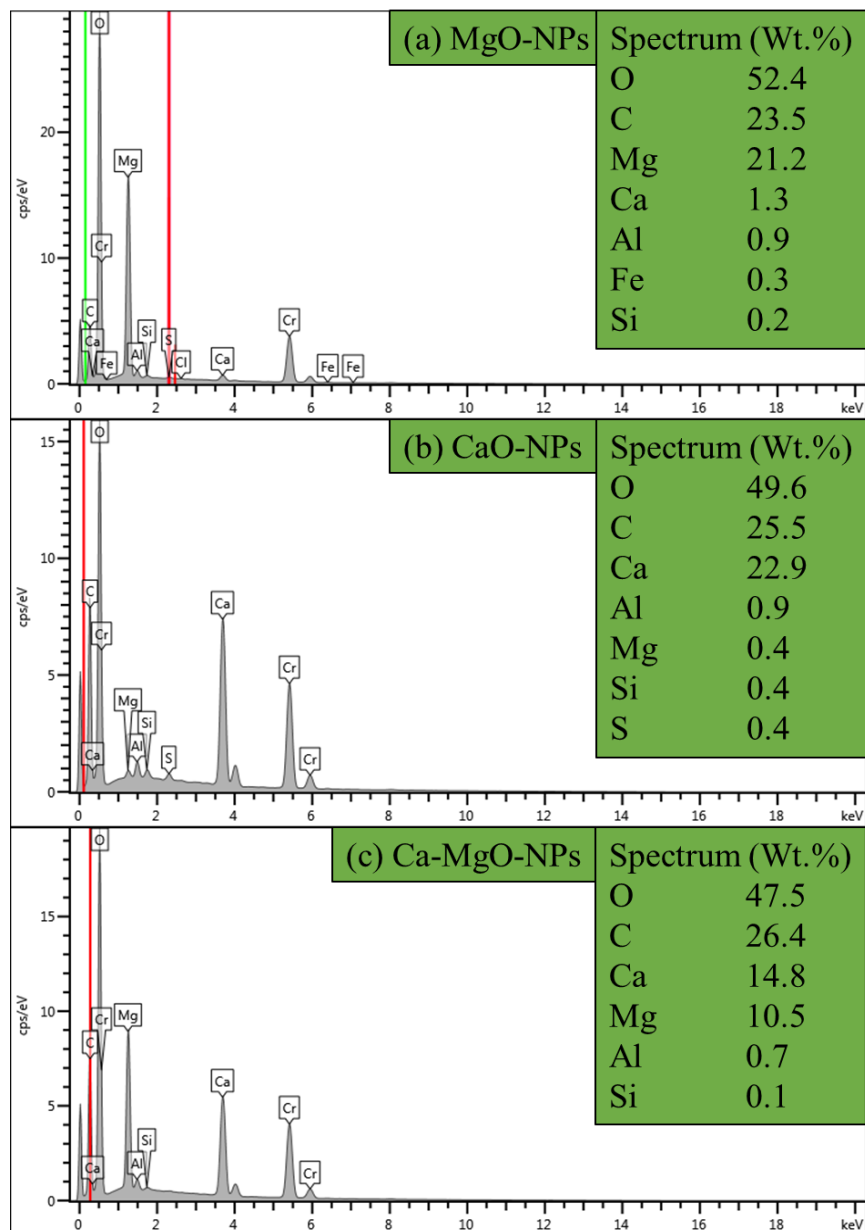
Fig.7. Elemental composition of MgO-NPs (a), CaO-NPs hydrated (b) and MgO-NPs-CaO-hydrous nanocomposite (c) as determined by EDX technique.

5. Characterization of feed and product minerals

5.1. Elemental composition from EDX

The elemental composition of MgO-NPs, CaO-NPs (hydrated lime), and MgO-NPs-CaO-hydrous nanocomposite via EDX is shown in Figure 7(a – c).

In Figure 7a, MgO-NPs were comprised of O, C, and Mg as major components; however, traces of Ca, Al, Fe, and Si were observed in the matrices. Mg and O were traced back to MgO. The CaO-NPs were comprised of O, C, and Ca as principal elements, with traces of Al, Mg, Si and S. Ca and O were traced back to the CaO-NPs hydrated (Figure 7b). Figure 7c indicates that the MgO-NPs-CaO-hydrous nanocomposite contained O, C, Ca, and Mg as the major chemical species and had traces of Al and Si on its matrices. The homogenization of CaO-NPs hydrated and MgO-NPs resulted in the co-distribution of elements. Essentially, the feed and product nanoparticles in Figure 7(a–c) were comprised of O, C, Ca and Mg as major elements, and this will play an indispensable role in increasing the pH of the product water, promoting the precipitation of Mn as a metal hydroxide. Similar claims have been elucidated in the literature [36,43,49]. The existence of O in the nanoparticles denoted (hydr) oxides formation. The presence of C (carbon) could be traced back to the material used for coating, which was utilized for the formation of a conductive layer in the samples examined. The Al, Fe, S and Si had lower concentrations, which were rooted in the aqueous solution. Due to minute levels of Mn, this element could not be detected in the product sludge.

5.2. Morphological characteristics from HR-SEM

The morphological characteristics of MgO-NPs, CaO-NPs (hydrated lime), and MgO-NPs-CaO-hydrous nanocomposite as determined by FIB-HR-SEM are shown in Figure 8(a – c). As shown in Figure 8(a – c), FIB-HR-SEM was utilized to determine the morphological characteristics of CaO-NPs hydrated, MgO-NPs, and their nanocomposite. As observed, clear images with high resolution were attained that show the morphological characteristics of the nanoparticles. As shown in Figure 8(a – b), the apparent variation in the morphologies of MgO-NPs and CaO-NPs hydrated utilized for the synthesis of the MgO-NPs-CaO-

hydrous nanocomposite lacked uniform particle size, denoting that the material was heterogeneous. Figure 8a reveals the presence of leafy-like structures that were dispersed throughout the surface. Figure 8b reveals the presence of spherical as well as leafy-like structures dispensed throughout the surface. A study performed by [51] confirmed lime to constitute leafy-like structures. In another study, the MgO-NPs were comprised of spherical structures, as reported by [52]. Thenceforth, in Figure 8c, it is clear that the MgO-NPs-CaO-hydrous nanocomposite was comprised of different morphological structures, including Mg, Ca, O, and C; these are the main elements of individual materials and were distributed evenly. This was also confirmed by the results obtained by EDX for elemental composition. Congruent distribution further confirmed that the materials were fully homogeneous.

5.3. Functional groups as ascertained by FTIR

The functional groups and wavenumbers for MgO-NPs, CaO-NPs (hydrated lime), and MgO-NPs-CaO-hydrous nanocomposite as determined by FTIR are shown in Figure 9(a – c). As indicated in Figure 9(a – c), the FTIR spectrums and functional groups with their corresponding wave numbers for CaO-NPs hydrated, MgO-NPs, and MgO-NPs-CaO-hydrous nanocomposite were captured. Interestingly, the peaks at 850 cm^{-1}, 1450 cm^{-1}, and 3650 cm^{-1} were observed to be the eminent peaks for both spectrums (Figure 9a). At 850 cm^{-1} and 1450 cm^{-1}, the spectrums contained the carbonate bond. Furthermore, at 3650 cm^{-1}, the spectrums showed strong absorbance peaks of -OH groups, confirming that the material was hydrated. [53] Reported -OH groups at 3696 – 3698 cm^{-1} and carbonates at 912 cm^{-1} and 1472 cm^{-1}. Findings from this study support the results obtained in this study. Figure 9b depicts the spectrums for MgO-NPs and that of the produced sludge. At 850 cm^{-1}, the carbonate bond was identified, while at 1450 cm^{-1}, the produced sludge comprised a weak bend. Specifically, the MgO-NPs showed strong symmetric and asymmetric stretching vibrations of carbonate. Water molecules were present for both spectrums, i.e., at 2950 cm^{-1}, whereas OH groups were observed at 3750 cm^{-1}. A study performed by [54] also indicated the presence of OH groups in

MgO-NPs, whereas [55] confirmed the presence of CO_3 bonds at 1430 – 1440 cm^{-1}. In Figure 9c, the MgO-NPs-CaO-hydrous nanocomposite and the produced sludge were comprised of carbonate bonds at 850 cm^{-1} and 1450 cm^{-1}. The water molecules were detected at 2950 and 3650 cm^{-1}, indicating that the material was hydrated. The peak at 1200 confirmed the Mn stretching [56].

6. Estimation of precipitation using PHREEQC geochemical model

Estimations and suggestions of chemical species that are more likely to precipitate from the interaction of CaO-NPs hydrated, MgO-NPs, and MgO-NPs-CaO-hydrous nanocomposite are summarized in Table 2. As shown in Table 2, different mineral phases were predicted to precipitate and their saturation index (SI). The saturation was mainly influenced by temperature and pH [57]. Specifically, Mn was observed to undergo precipitation as birnessite, bixbyite, nsutite, rhodochrosite, hausmannite, manganite, pyrolusite, and rhodochrosite. Carbonate species of dolomite and calcite were also observed, which corroborated the FTIR results. Hausmannite had the highest saturation index. All minerals were oversaturated (SI > 0), and therefore precipitation could take place.

7. Mechanisms governing the removal of manganese from drinking water

The used chemicals are not adsorbent primarily due to their high aqueous solubility nature; as such, they partially dissolve in water due to the presence of soluble parts (fractions) and non-soluble fractions. As they dissolved in water, they increased the pH of the water through the addition of hydroxyl groups (OH$^-$) (Eqn. 2-3), thus promoting the precipitation of manganese as birnessite, bixbyite, nsutite, rhodochrosite, hausmannite,

manganite, pyrolusite, and rhodochrosite as predicted by PHREEQC geochemical simulations and complemented by analytical techniques. After contacting the water, the level of alkali and earth alkali metals increased in the aqueous solution (Table 1), indicating a possible dissolution of base cations leading to an increase in pH (Eqn. 2 and 3) and a possible precipitation of metal species as hydroxide (Eqn. 4-6). The dissolution of base cations may be represented by the following equations [58]:

$$MgO + H_2O \rightarrow Mg^{2+} + 2OH^- \qquad (2)$$

$$CaO + H_2O \rightarrow Ca^{2+} + 2OH^- \qquad (3)$$

The individual materials (MgO and CaO, although supplied in a more stable hydroxyl form) and their derivative composite with calcined dolomitic properties will lead to the formation of hydroxyl groups and an increase in Mg^{2+} and Ca^{2+} levels in the aqueous solution [59,60]. An increase in pH shifts the paradigm of the equilibrium state of the aqueous system, fostering the precipitation of manganese as hydroxides (Eqn. 4-6).

$$M^{n+} + nOH^- \rightarrow M(OH)_n \downarrow \qquad (4)$$

$$Mn^{2+} + OH^- \rightarrow Mn(OH)_{2(s)} \downarrow \qquad (5)$$

$$Mn^{2+} + H_2O \rightarrow Mn(OH)_{2(s)} + H^+ \qquad (6)$$
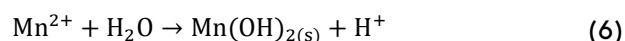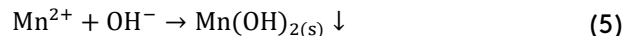
An increase in the pH of the product water may also be due to dissolution of fractions from the feed material, as shown by FTIR and EDS and the release of Mg, Ca and Na, as revealed by the EDS technique. The hydration of the product mineral denotes the formation of metal hydroxide, i.e., Mn(OH)$_2$. In essence, the principal mechanism that is predicted for the removal of Mn and other contaminants in aqueous solution is precipitation, although co-precipitation and co-adsorption could prevail to the formed sludge.

Table 2. Estimations and suggestions of chemical species that are more likely to precipitate from the interaction of CaO-NPs hydrated, MgO-NPs, and MgO-NPs-CaO-hydrous nanocomposite.

Mineral name	SI	Chemical name	Mineral name	SI	Chemical name
Birnessite	7.18	MnO_2	Hausmannite	19.70	Mn_3O_4
Bixbyite	15.35	Mn_2O_3	Manganite	7.54	MnOOH
Nsutite	8.22	MnO_2	Pyrolusite	9.40	MnO_2
Rhodochrosite	2.72	$MnCO_3$	Rhodochrosite(d)	1.98	$MnCO_3$
Dolomite	0.19	$CaMg(CO_3)_2$	Calcite	0.00	$CaCO_3$
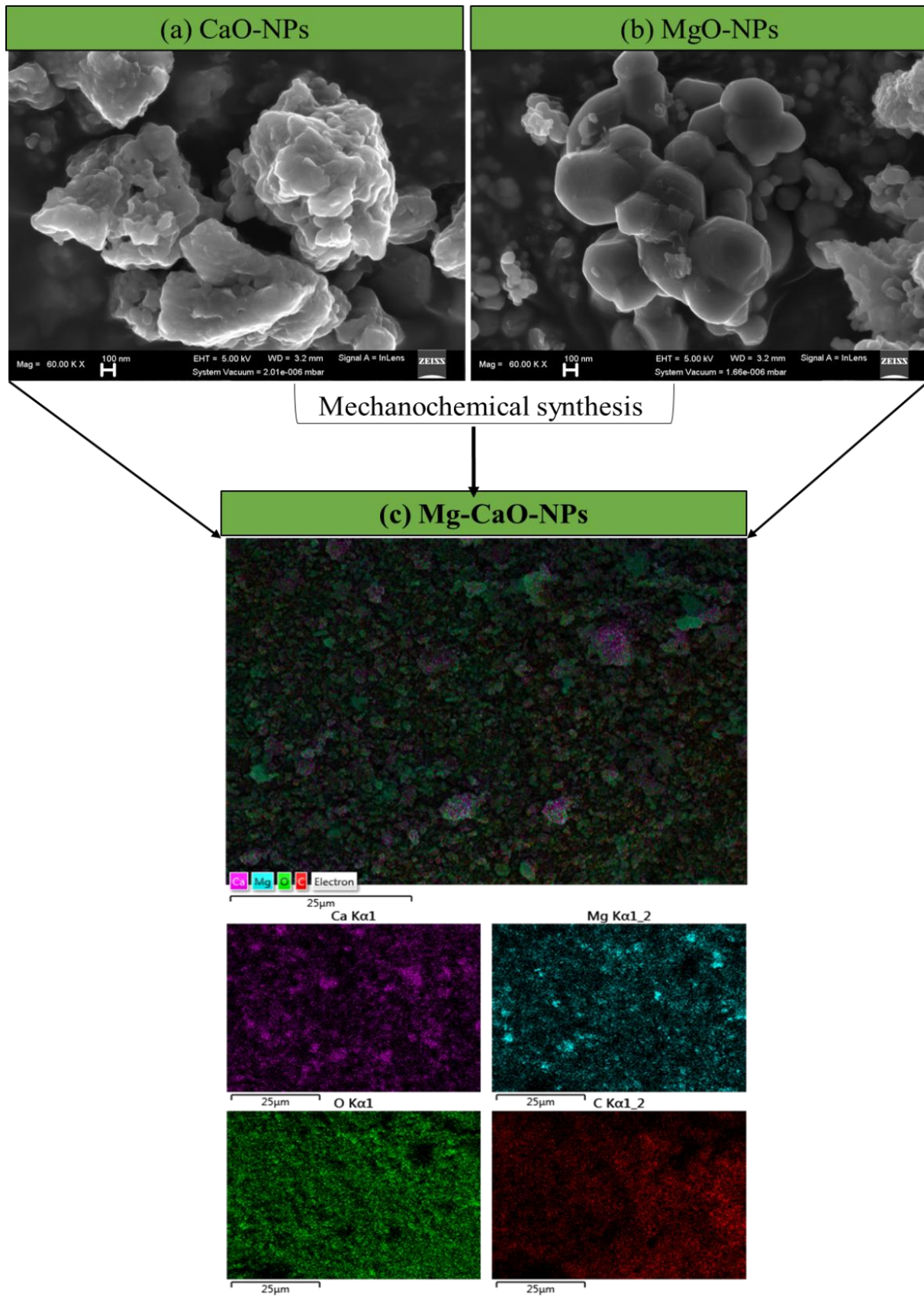
Fig. 8. The morphological characteristics of MgO-NPs, CaO-NPs (hydrated lime), and MgO-NPs-CaO-hydrous nanocomposite as determined by FIB-HR-SEM.

8. Conclusions

This study successfully demonstrated the feasibility of the mechanochemical synthesis of the MgO-NPs-CaO-hydrous nanocomposite via vibratory ball milling and calcination. The efficacy of the synthesized nanocomposite was evaluated on the removal of Mn from aqueous solution. Specifically, the optimum conditions were observed to be 15 min of mixing, 0.5 g of dosage, and 200 rpm of mixing speed. The interaction of the hydrated lime, MgO-NPs, and MgO-NPs-CaO-hydrous nanocomposite with Mn-rich aqueous solution led to an increase in the pH and registered in a sequence of ≥11.78, ≥10.17, and ≥11.35, respectively. The Mn removal efficiency was registered as ≥72.4%, ≥91.8%, and ≥83% for hydrated lime, MgO-NPs, and MgO-NPs-CaO-hydrous nanocomposite, respectively. Their respective turbidities were ≤0.41 NTU, ≤3.50 NTU, and ≤1.05 NTU. An increase in pH contributed significantly to the removal of Mn as a different chemical species, i.e., birnessite, hausmannite, bixbyite, manganite, nsutite, pyrolusite, and rhodochrosite. Finally, the Ca^{2+}, Mg^{2+}, and Mn^{2+} were predicted to exist as divalent species in the aqueous solution. As expected, the MgO-NPs-CaO-hydrous nanocomposite demonstrated superior performance compared to individual materials, and the synergistic effects and complementary behavior could explain this. As such, findings from this study confirmed the effectiveness of the MgO-NPs-CaO-hydrous nanocomposite and its derivatives in removing Mn from real river water. Findings from this study will go a long way in curtailing the aesthetic and health impacts of Mn in drinking water and further afield. The study results can guide water treatment entities regarding the most effective way to manage Mn in raw water and curtail distribution challenges.

Acknowledgments

References

[1] Fayazi, M., Afzali, D., Ghanei-Motlagh, R., Iraji, A. (2019). Synthesis of novel sepiolite–iron oxide–manganese dioxide nanocomposite and application for lead(II) removal from aqueous solutions. *Environmental science and pollution research journal*, *26*(18), 18893-18903

[2] Lee, I., Hwang, H, Lee, J, Yu, N, Yun, J Kim, H. (2017). Modeling approach to evaluation of environmental impacts on river water quality: a case study with Galing River, Kuantan, Pahang, Malaysia. *Journal of ecological modelling, 353*, 167-173.

[3] Jin, W., Du, H, Zheng, S Zhang, Y. (2016). Electrochemical processes for the environmental remediation of toxic Cr (VI): A review. *Electrochimica acta journal, 191*, 1044-1055.

[4] Fayazi, M. (2020). Removal of mercury (II) from wastewater using a new and effective composite: sulfur-coated magnetic carbon nanotubes. *Environmental science and pollution research*, *27*(11), 12270-12279.

[5] Zhao, M., Xu, Y., Zhang, C, Rong, H Zeng, G. (2016). New trends in removing heavy metals from wastewater. *Applied microbiology and biotechnology journal, 100*(15), 6509-6518.

[6] Zou, Y., Wang, X, Khan, A, Wang, P, Liu, Y Alsaedi, A. (2016). Environmental remediation and application of nanoscale zero-valent iron and its composites for the removal of heavy metal ions: a review. *Journal of environmental science and technology, 50*(14), 7290-7304.

[7] Neculita, C. M., Rosa, E. (2019). A review of the implications and challenges of manganese removal from mine drainage. *Chemosphere journal, 214*, 491-510.

[8] WHO. (2004). *Manganese in drinking water: background document for development of WHO Guidelines for drinking-water quality*.

[9] Gerke, T., Little, BJ and Barry Maynard, J. (2015). Manganese deposition in drinking water distribution systems. *Science of total environment journal, 541*, 184-193.

[10] Idrees, N., Tabassum, B., Abd_Allah, E. F., Hashem, A., Sarah, R., Hashim, M. (2018). Groundwater contamination with cadmium concentrations in some West UP Regions,

India. *Saudi journal of biological sciences, 25*(7), 1365-1368.

[11] Neshat, A., Oghazyan, A., Kariminejad, F., Mahmudiono, T., Fakhri, Y., Asadi, A. M. SKhaneghah, A. M. (2022). The concentration of potentially toxic elements (PTEs) in human milk: a systematic review, meta-analysis, and health risk assessment. *Journal of food composition and analysis*, 104933.

[12] Mthombeni, N. H., Mbakop, S., Onyango, M. S. (2022, April). Adsorptive removal of manganese from industrial and mining wastewater. In *proceedings of the sustainable research and innovation conference* (pp. 36-45).

[13] Tobiason, J. E., Bazilio, A., Goodwill, J., Mai, X., Nguyen, C. (2016). Manganese removal from drinking water sources. *Journal of current pollution reports, 2*(3), 168-177.

[14] Canada, H. (2016). *Manganese in drinking water* (Document for public consultation, Prepared by the federal-provinvial-territorial committee for drinking water, Issue.

[15] Adams, B., Anderson, R., Bless, D., Butler, B., Conway, B., Dailey, A., Freed, E., Gervais, G., Gill, M., Grosse, D. (2014). Reference guide to Treatment Technologies for mining-influenced water. *Washington, USA: US environmental protection Agency-OSRTI*, 8-30.

[16] Favas, P. J. C., Sarkar, S. K., Rakshit, D., Venkatachalam, P., Prasad, M. N. V. (2016). Acid mine drainages from abandoned mines: hydrochemistry, environmental impact, resource recovery, and prevention of pollution. In *Environmental materials and waste* (pp. 413-462). Academic Press.

[17] Patil, D., Chavan, S., Oubagaranadin, J. (2016). A review of tehnologies for manganese removal from wastewater. *Environmental chemical engineering journal, 4*(1), 468-487.

[18] Rudi, N. N., Muhamad, M. S., Te Chuan, L., Alipal, J., Omar, S., Hamidon, N., Hamid, N. H. A., Sunar, N. M., Ali, R., Harun, H. (2020). Evolution of adsorption process for manganese removal in water via agricultural waste adsorbents. *Heliyon journal, 6*(9), e05049.

[19] Gunatilake, S. (2015). Methods of removing heavy metals from industrial wastewater. *Methods journal, 1*(1), 14.

[20] Shirmohammadi, E., Khaje, M., Shirdali, M., Hosein, G., Shahgholi, H. (2014). Microorganisms's application strategy for bio-phytoremediation of heavy metal: a review. *Biodiversity and environmental sciences journal, 5*, 289-298.

[21] Myasnikov, S., Tikhonov, A., Chipryakova, A., Kulov, N. (2016). Removal of heavy metal ions from water by an combined sorption-crystallization process using activated clays. *Theoretical foundations of chemical engineering journal, 50*(4), 366-382.

[22] Fayazi, M., Ghanbarian, M. (2020). One-pot hydrothermal synthesis of polyethylenimine functionalized magnetic clay for efficient removal of noxious Cr (VI) from aqueous solutions. *Silicon, 12*(1), 125-134.

[23] Aguiar, A., Xavier, G., Ladeira, A. (2010, May). The use of limestone, lime and MnO2 in the removal of soluble manganese from acid mine drainage. In *10th International conference of water pollution: modelling, monitoring and management* (pp. 267-276).

[24] Mulyadi, D., Haryati, S., Said, M. (2020). The effect of calcium oxide and aluminum sulfate on iron, manganese and color removal at peat water treatment. *Indonesian journal of fundamental and applied chemistry, 5*(2), 42-48.

[25] Cortina, J. L., Lagreca, I., De Pablo, J., Cama, J., Ayora, C. (2003). Passive in situ remediation of metal-polluted water with caustic magnesia: evidence from column experiments. *Environmental science and technology, 37*(9), 1971-1977.

[26] Charerntanyarak, L. (1999). Heavy metals removal by chemical coagulation and precipitation. *Water science and technology journal, 39*(10-11), 135-138.

[27] Chen, B., Qu, R., Shi, J., Li, D., Wei, Z., Yang, X., & Wang, Z. (2011). Heavy metal and phosphorus removal from waters by optimizing use of calcium hydroxide and risk assessment. *Environment and pollution journal, 1*(1), 38.

[28] Masindi, V., Ndiritu, J. G., Maree, J. P. (2018). Fractional and step-wise recovery of chemical species from acid mine drainage using calcined cryptocrystalline magnesite nano-sheets: An experimental and geochemical modelling

approach. *Journal of environmental chemical engineering, 6*(2), 1634-1650.

[29] Schiller, J., Tallman, D., Khalafalla, S. (1984). Mineral processing water treatment using magnesium oxide. *Environmental progress journal, 3*(2), 6.

[30] Masindi, V., Gitari, M. W., Tutu, H., DeBeer, M. (2017). Synthesis of cryptocrystalline magnesite–bentonite clay composite and its application for neutralization and attenuation of inorganic contaminants in acidic and metalliferous mine drainage. *Journal of water process engineering, 15*, 2-17.

[31] Tran, H. N., You, S. J., Hosseini-Bandegharaei, A., Chao, H. P. (2017). Mistakes and inconsistencies regarding adsorption of contaminants from aqueous solutions: A critical review. *Water research, 120*, 88-116.

[32] Parkhurst, D. L., Appelo, C. (2013). Description of input and examples for PHREEQC version 3—a computer program for speciation, batch-reaction, one-dimensional transport, and inverse geochemical calculations. *US geological survey techniques and methods, 6*(A43), 497.

[33] Parkhurst, D. L., Appelo, C. (1999). User's guide to PHREEQC (Version 2): A computer program for speciation, batch-reaction, one-dimensional transport, and inverse geochemical calculations. *Water-resources investigations report, 99*(4259), 312.

[34] Choi, H., Woo, N. C., Jang, M., Cannon, F. S., Snyder, S. A. (2014). Magnesium oxide impregnated polyurethane to remove high levels of manganese cations from water. *Separation and purification technology journal, 136*, 184-189.

[35] Bamforth, S. M., Manning, D. A., Singleton, I., Younger, P. L., Johnson, K. L. (2006). Manganese removal from mine waters–investigating the occurrence and importance of manganese carbonates. *Applied geochemistry journal, 21*(8), 1274-1287.

[36] Masindi, V., Foteinis, S., Chatzisymeon, E. (2022). Co-treatment of acid mine drainage and municipal wastewater effluents: Emphasis on the fate and partitioning of chemical contaminants. *Journal of hazardous materials, 421*, 126677.

[37] Masindi, V., Foteinis, S., Renforth, P., Ndiritu, J., Maree, J. P., Tekere, M., Chatzisymeon, E. (2022). Challenges and avenues for acid mine drainage treatment, beneficiation, and valorisation in circular economy: A review. *Ecological engineering, 183*, 106740.

[38] Orescanin, V., Ruk, D., Kollar, R., Mikelic, I. L., Nad, K., Mikulic, N. (2011). A combined treatment of landfill leachate using calcium oxide, ferric chloride and clinoptilolite. *Journal of environmental science and health part A, 46*, 323-328.

[39] Rout, C., Sharma, A. (2011). Assessment of drinking water quality: A case study of Ambala cantonment area, Haryana, India. *International journal of environmental sciences, 2*(2), 933-945.

[40] Masindi, V., Fosso-Kankeu, E., Mamakoa, E., Nkambule, T. T. I., Mamba, B. B., Naushad, M., Pandey, S. (2022). Emerging remediation potentiality of struvite developed from municipal wastewater for the treatment of acid mine drainage. *Environmental research, 210*, 112944.

[41] Akinwekomi, V., Maree, J. P., Zvinowanda, C., Masindi, V. (2017). Synthesis of magnetite from iron-rich mine water using sodium carbonate. *Journal of environmental chemical engineering, 5*(3), 2699-2707.

[42] Akinwekomi, V., Maree, J. P., Masindi, V., Zvinowanda, C., Osman, M. S., Foteinis, S., Mpenyana-Monyatsi, L., Chatzisymeon, E. (2020). Beneficiation of acid mine drainage (AMD): A viable option for the synthesis of goethite, hematite, magnetite, and gypsum – Gearing towards a circular economy concept. *Minerals engineering, 148*, 106204.

[43] Kefeni, K. K., Msagati, T. A. M., Mamba, B. B. (2017). Acid mine drainage: Prevention, treatment options, and resource recovery: A review. *Journal of cleaner production, 151*, 475-493.

[44] Lei, X., Shimada, S., Intabon, K., Maekawa, T. (2006). Pretreatment of methane fermentation effluent by physico-chemical processes before applied to soil trench system. *Agricultural engineering international: the CIGR ejournal, 8*.

[45] Simate, G. S., Ndlovu, S. (2014). Acid mine drainage: Challenges and opportunities. *Journal of environmental chemical engineering, 2*(3), 1785-1803.

[46] Park, I., Tabelin, C. B., Jeon, S., Li, X., Seno, K., Ito, M., Hiroyoshi, N. (2019). A review of recent strategies for acid mine drainage prevention and mine tailings recycling. *Chemosphere journal, 219*, 588-606.

[47] Naidu, G., Ryu, S., Thiruvenkatachari, R., Choi, Y., Jeong, S., Vigneswaran, S. (2019). A critical review on remediation, reuse, and resource recovery from acid mine drainage. *Environmental pollution, 247*, 1110-1124.

[48] Masindi, V., Foteinis, S., Renforth, P., Ndiritu, J., Maree, J. P., Tekere, M., Chatzisymeon, E. (2022). Challenges and avenues for acid mine drainage treatment, beneficiation, and valorisation in circular economy: A review. *Ecological engineering*, *183*, 106740.

[49] Masindi, V., Akinwekomi, V., Maree, J. P., Muedi, K. L. (2017). Comparison of mine water neutralisation efficiencies of different alkaline generating agents. *Journal of environmental chemical engineering, 5*(4), 3903-3913.

[50] Chen, G., Ye, Y., Yao, N., Hu, N., Zhang, J., Huang, Y. (2021). A critical review of prevention, treatment, reuse, and resource recovery from acid mine drainage. *Journal of cleaner production, 329*, 129666.

[51] Masindi, V., Osman, M., Abu-Mahfouz, A. (2017). Integrated treatment of acid mine drainage using BOF slag, lime/soda ash and reverse osmosis (RO): Implication for the production of drinking water. *Desalination journal, 424*, 45-52.

[52] Yu, J., Xu, A., Zhang, L., Song, R., Wu, L. (2004). Synthesis and characterization of porous magnesium hydroxide and oxide nanoplates. *Physical chemistry journal, 108*, 64-70.

[53] Hwidi, R. S., Izhar, T. N. T., Saad, F. N. M., Dahham, O. S., Noriman, N. Z., Shayfull, Z. (2018, November). Characterization of quicklime as raw material to hydrated lime: effect of temperature on its characteristics. In *AIP conference proceedings* (Vol. 2030, No. 1, p. 020027). AIP publishing LLC.

[54] Kandiban, M., Vigneshwaran, P., Potheher, I. V. (2015, January). Synthesis and characterization of mgo nanoparticles for photocatalytic applications. In *department of physics, Bharathidasan institute of technology (BIT) Campus, Anna University, Tiruchirappalli, Tamilnadu, India, conference paper*.

[55] Selvam, N. C. S., Kumar, R. T., Kennedy, L. J., Vijaya, J. J. (2011). Comparative study of microwave and conventional methods for the preparation and optical properties of novel MgO-micro and nano-structures. *Alloys and compounds journal, 509*, 9809-9815.

[56] Kang, L., Zhang, M., Liu, Z. H., Ooi, K. (2007). IR spectra of manganese oxide with either layered or tunnel structures. *Journal of spectrochimica acta part A, 67*, 864-869.

[57] Stumm, W. (1997). Reactivity at the mineral-water interface: dissolution and inhibition. *Colloids and surfaces A: physicochemical and engineering aspects journal, 120*(1-3), 143-166.

[58] Masindi, V., Gitari, M. W., Tutu, H., & DeBeer, M. (2017). Synthesis of cryptocrystalline magnesite–bentonite clay composite and its application for neutralization and attenuation of inorganic contaminants in acidic and metalliferous mine drainage. *Journal of water process engineering*, *15*, 2-17.

[59] Pishtshev, A., Karazhanov, S. Z., Klopov, M. (2014). Material properties of magnesium and calcium hydroxides from first-principles calculations. *Computational materials science journal, 95*, 693 - 705.

[60] Rotting, T. S., Cama, J., Ayora, C., Cortina, J. L., De Pablo, J. (2006). Use of caustic magnesia to remove cadmium, nickel and cobalt from water in passive treatment systems: Column experiments. *Environmental science and technology journal, 40*, 6438 - 6443.